

MICROSTRUCTURE EVOLUTION MODEL FOR THE HAZ OF GIRTH WELDS IN X80 LINEPIPE STEEL

M. Militzer, M. Maalekian, T. Garcin and W.J. Poole

The Centre for Metallurgical Process Engineering, The University of British Columbia,
Vancouver, BC, Canada V6T 1Z4

Keywords: X80 Linepipe, Girth Welding, Microstructure Model, HAZ

Abstract

A phenomenological model has been developed to describe austenite grain growth, precipitate dissolution and austenite decomposition into ferrite, bainite and martensite/austenite (MA) constituents for an X80 linepipe steel. The predictive capabilities of the integrated model for the heat affected zone (HAZ) have been validated with laboratory simulations of heat treatment cycles for selected positions in the HAZ. The model predicts the fraction of transformation products as a function of distance from the fusion line. To connect the microstructure model to a mechanical property model for the HAZ it will be required to incorporate a module on MA island size as this is expected to critically affect the fracture toughness.

Introduction

Microstructure engineering has gained increasing attention over the past decades as a process modelling tool for hot rolling and heat treatment of steels [1]. In this modelling concept, the operational parameters of an industrial process are related to the properties of the product material by accurately modelling the microstructure evolution during the thermo-mechanical processing path. Microstructure process models for the weld heat affected zone (HAZ) have been proposed with an emphasis on austenite grain growth [2, 3]. The austenite grain size provides the initial condition for subsequent phase transformation during cooling [4, 5]. Large austenite grain sizes are of particular concern during welding where the HAZ experiences rapid thermal cycles with high peak temperatures, especially in the region adjacent to the fusion zone. In general, martensite formation in the HAZ is a concern as it may lower the weld toughness and increase the risk of hydrogen cracking [6-11]. It also increases the vulnerability to cold cracking and reheat cracking in welds. Further, the grain structure in the HAZ influences the grain size in the weld metal where the grains grow epitaxially from the HAZ [6].

In the HAZ, austenite formation and grain growth occur during rapid heating with heating rates in the order of 1000 °C/s. A number of attempts have been made to study the effect of heating rate and more complex non-isothermal heat treatment cycles on austenite grain growth kinetics, as summarized in the extensive review of non-isothermal grain growth by Mishra and DebRoy [12]. A particular focus on modelling austenite grain growth in the HAZ has recently been on microalloyed steels (e.g. linepipe grades) where grain growth is affected by the presence of precipitates and their potential dissolution and coarsening [2, 3]. By investigating isothermal austenite grain growth and particle coarsening behaviour, Moon et al. [13] quantified the effects of particles on grain boundary pinning and alloying elements on grain boundary mobility. Employing the additivity rule, austenite grain growth was simulated for the non-isothermal

conditions in the weld HAZ of a Ti-microalloyed steel. Based on elementary kinetic models for grain growth and carbide dissolution integrated over the weld cycle, Ashby and Easterling [10] proposed grain growth diagrams for steel welding by fitting the unknown kinetic constants to data from real or simulated welds. Their analytical model was further improved by incorporating precipitate coarsening. Andersen and Grong [14] proposed an extensive analytical model of grain growth in the presence of growing and dissolving precipitates. They presented their results in the form of mechanism maps which show the competition between the various processes during grain growth in conjunction with coarsening or dissolution of precipitates. Further, a substantial body of work exists to connect the austenitizing condition to the subsequent austenite decomposition in the HAZ. The majority of the microstructure evolution modelling work in both weld metal and HAZ regions can be traced to three seminal contributions by Ashby and Easterling [10], Henwood et al. [15] and Bhadeshia et al. [16]. More recently, these approaches have been extended to account for complex microstructure evolution in steel welds [17]. The classic textbook by Grong provides an extensive overview on calculation methodologies and modelling tools related to microstructure evolution during welding [18]. Recently, Zhang et al. [19] investigated the microstructure evolution in the HAZ of a low carbon steel during gas tungsten arc welding using a combination of several numerical models. In particular, the ferrite to austenite phase transformation was described using a Johnson-Mehl-Avrami-Kolgomorov (JMAK) analysis, the austenite grain growth was calculated with a Monte Carlo simulation and the transformation of austenite to various transformation products during cooling was simulated using the austenite decomposition model proposed by Bhadeshia et al. [16, 20]. Thiessen et al. [21] considered the phase transformation kinetics and resulting microstructures at various positions in the HAZ of selected advanced low carbon steels. They obtained good agreement with experimental data by using a phase field model with a number of adjustable parameters for nucleation and growth rates (e.g. interface mobility).

These modelling approaches for the HAZ do not exploit the full potential of the microstructure engineering concept as they do not combine (a) the time-temperature path as a function of the weld parameters, (b) the associated microstructure evolution and (c) the relation between the final microstructure and the properties of the HAZ. We have designed a research program to develop an integrated microstructure-property model for the HAZ of girth welds in linepipe steels. The results on austenite grain growth in a Ti-Nb microalloyed X80 linepipe steel were recently published including a combined model for grain growth and precipitate dissolution [2, 3]. Similarly, we reported results on austenite decomposition and initial model concepts for describing transformation temperatures as a function of cooling path, austenite grain size and amount of Nb in solution in the investigated steel [22, 23]. The aim of the present paper is to provide an integrated microstructure model for the HAZ of the investigated X80 linepipe steel. The predictive capabilities of the proposed model are evaluated with dedicated validation experiments for typical heat treatment cycles in the HAZ. The model presented here only considers the portion of the HAZ that experiences full austenitization.

Modelling Approach

The development of the microstructure evolution model follows the well established concept of conducting systematic austenite grain growth and austenite decomposition studies in the laboratory for process conditions of industrial relevance. Here, an X80 linepipe steel was selected for these investigations. The chemistry of this steel is shown in Table I. All laboratory

simulations were conducted on a Gleeble 3500 thermo-mechanical simulator as described elsewhere in detail [2, 22, 23]. A first series of experiments consisted of systematic continuous heating and cooling tests to aid the development of phenomenological microstructure evolution models for the HAZ. In particular, a set of material specific parameters was determined from these tests. Heating tests with heating rates of 10, 100 and 1000 °C/s to austenitizing temperatures in the range of 900 to 1350 °C were employed to quantify austenite grain growth [2]. Continuous cooling tests were conducted at cooling rates of 1 to 100 °C/s with a variety of austenitizing conditions to systematically change the austenite grain size (5 – 80 µm) and the level of Nb in solution. The latter was controlled by a variation of holding times at 900 °C to facilitate various degrees of Nb re-precipitation after having put Nb fully into solid solution [22].

A second series of Gleeble simulations was conducted to validate the predictive capabilities of the models for their application to the HAZ. For this purpose, suitable time-temperature paths for the simulations were obtained using potential HAZ thermal cycles according to the Rosenthal equation for thick plates.

Table I. Steel Chemistry (key elements in wt.%)

C	Mn	Nb	Ti	Mo	N
0.06	1.65	0.034	0.012	0.24	0.005

Model Formulation

Austenite Grain Growth

Detailed experimental studies were conducted to determine austenite formation and austenite grain growth kinetics during rapid heat treatment scenarios [2]. These investigations also included in-situ measurements of the grain size evolution by laser ultrasonics [3]. Based on these experimental observations, a combined austenite grain growth and precipitate dissolution model has been proposed that is briefly summarized below. In the investigated steel microalloyed with Nb and Ti (see Table I), four types of precipitates were observed in the base metal, i.e. Mo carbides, Ti nitrides as well as fine (< 5 nm) and coarse (> 10 nm) Nb carbonitrides. Analysis of their equilibrium solubilities suggests that Mo is completely in solution before ferrite starts to transform to austenite whereas Ti remains almost completely precipitated even at the melting temperature. On the other hand, Nb precipitates are expected to completely dissolve above 1150 °C in the present steel. Grain growth is significantly affected by the presence of these precipitates which can provide grain boundary pinning. Thus, an austenite grain growth model for the HAZ must account for the potential dissolution of precipitates and the associated changes in the pinning force. Further, the amount of Nb in solution will also significantly affect the subsequent austenite decomposition kinetics [22, 23]. For simplicity, it is assumed that TiN remains stable throughout any heat treatment cycle in the HAZ and the Nb precipitates are approximated as NbC. Further, the austenite formation is completed at 910 °C for a heating rate of 1000 °C/s [2]. The typical austenite grain size of 4 µm that was observed at this stage can be taken as initial grain size in the grain growth model.

The evolution of the mean austenite grain size, d_γ , can be described as:

$$\frac{d(d_\gamma)}{dt} = M\gamma \left(a \frac{1}{d_\gamma} - P_p \right) \quad (1)$$

where γ is the grain boundary energy, a is a geometrical constant, P_p is the pinning parameter and M is the grain boundary mobility that is usually given by an Arrhenius relationship, i.e.:

$$M = M_0 \exp\left(-\frac{Q}{RT}\right) \quad (2)$$

where M_0 is a pre-exponential term, Q is an effective activation energy, R is the gas constant and T is the absolute temperature. The pinning parameter can be written as:

$$P_p = b \sum_i^N \frac{f_i}{r_i} \quad (3)$$

for a population of N precipitate families i with volume fractions f_i and mean particle radii r_i ; b is another geometric constant. The dissolution kinetics of NbC can be described by:

$$\frac{dr_j}{dt} = \frac{D}{r_j} \frac{X - X_{Nb}^j(r_j)}{v_{at}^M X^P / v_{at}^P - X_{Nb}^j(r_j)} \quad (4)$$

where j is introduced to indicate the two NbC precipitate types, i.e. small (s) and large (l), respectively. D is the diffusivity of the rate controlling element (i.e. here Nb), X is the mean solute mole fraction of Nb in the matrix, X_{Nb}^j is the equilibrium solute mole fraction of Nb at the precipitate/matrix interface, X^P is the mole fraction of Nb in the precipitate, $v_{at}^M = 1.1775 \times 10^{-29} \text{ m}^3$ and $v_{at}^P = 1.110 \times 10^{-29} \text{ m}^3$ are the atomic volume of matrix and NbC precipitates (i.e. mean volume per atom), respectively. Interface curvature plays an important role on equilibrium mole fraction, i.e. the so-called Gibbs-Thomson effect, and the equilibrium solubility depends on particle radius, r_j , and the matrix/precipitate interface energy, σ , such that [24]:

$$X_{Nb}^j(r_j) X_C = K_{\text{NbC}} \exp\left(\frac{4\sigma v_{at}^P}{r_j k_B T}\right) \quad (5)$$

Here, k_B is the Boltzmann constant, X_C is the equilibrium solute mole fraction of C at the precipitate/matrix interface and K_{NbC} is the solubility product. The initial volume fractions and mean particle sizes are provided in Table II. These data were obtained from an analysis of the precipitate population in the base metal and the resulting austenite grain growth behavior [3].

Table II. Initial Volume Fractions and Mean Radii of Precipitates [3]

Precipitate	Volume fraction ($\times 10^{-4}$)	Mean radius (nm)
TiN	2.2	38
NbC (large)	2.8	24
NbC (small)	1.0	3.5

Literature data are available for all model parameters in Equations (1) to (5) except M_o as summarized in Table III. A value of $M_o = 120 \text{ m}^4/\text{Js}$ was adopted to provide an adequate description of austenite grain growth during heating as illustrated in Figure 1. An important outcome of this model is that both the mean austenite grain size and the amount of Nb in solution are predicted along the thermal path in the austenite region.

Table III. Parameters for Combined Grain Growth – Dissolution Model

Parameter	Value	Reference
$\gamma (\text{J}/\text{m}^2)$	0.5	[25]
a	4	[26]
b	12	[27]
$Q (\text{kJ}/\text{mol})$	350	[28]
$\sigma (\text{J}/\text{m}^2)$	0.66	[3]
$D (\text{cm}^2/\text{s})$	$4.2 \exp\left(-\frac{286 \text{ kJ} / \text{mol}}{RT}\right)$	[29]
$\log_{10}(K_{\text{NbC}})$	$4.55 - 10345/T$	[30]

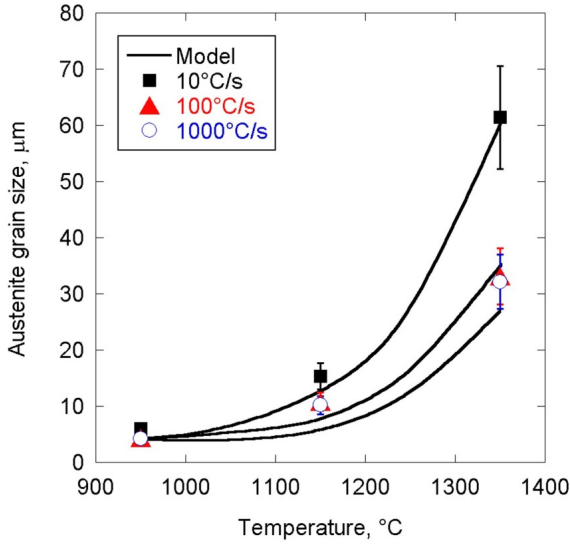


Figure 1. Measured and calculated austenite grain growth during continuous heating in the investigated X80 linepipe steel; holding times at peak temperatures are 0.5 s.

Austenite Decomposition

The austenite decomposition kinetics have been quantified as a function of austenitizing condition (i.e. austenite grain size and amount of Nb in solution) and cooling rate, as described elsewhere in more detail [22, 23]. Based on these studies a sequential transformation model is proposed with five sub-models for: (i) ferrite start temperature, (ii) ferrite growth kinetics, (iii) bainite start temperature, (iv) bainite growth kinetics, (v) martensite/austenite (MA) fraction.

To describe the transformation start temperature of ferrite a model previously proposed for plain low carbon steels has been adopted [31]. The model considers early carbon diffusion controlled growth of ferrite grains nucleated at austenite grain corners at a temperature, T_N . The original model was extended to include the drag effect of Nb that slows down the growth rate of ferrite. The modified growth rate equation can be formulated as [32]:

$$\frac{dR_f}{dt} = D_C \frac{C^\gamma - C_o}{C^\gamma - C^\alpha} \frac{1}{R_f} \left(1 + \frac{D_C \alpha C_{Nb}}{R_f} \right)^{-1} \quad (6)$$

where R_f is the radius of the growing ferrite grain, D_C is the carbon diffusivity in austenite [33], C_o is the average carbon concentration, C^α and C^γ are the carbon equilibrium concentrations in ferrite and austenite, respectively, C_{Nb} denotes the concentration of Nb in solution and α is a

constant related to the intensity of the solute-interface interaction. The carbon equilibrium concentrations are calculated with Thermo-Calc using the Fe2000 data base and assuming ortho-equilibrium (i.e. full equilibrium for all alloying elements). Measurable transformation start (i.e. 5% transformed) is assumed to be associated with nucleation site saturation at other grain boundary sites. Ferrite nucleation is presumed to cease once the carbon enrichment of the entire grain boundary area attains a critical level, C^* , i.e.:

$$R_f > \frac{1}{\sqrt{2}} \frac{C^* - C_o}{C^\gamma - C_o} d_\gamma \quad (7)$$

is the condition to calculate the transformation start temperature, T_s . The three adjustable parameters, i.e. T_N , C^* and α , have been determined from the experimental ferrite transformation start temperatures as summarized in Table IV. Figure 2 compares calculated with measured ferrite transformation start temperatures.

Table IV. Ferrite Transformation Start Parameters

T_N (°C)	C^*/C_o	α (s/ μm)/(at.ppm)
700	$1.74 + 6.8 \mu\text{m}/d_\gamma$	0.043

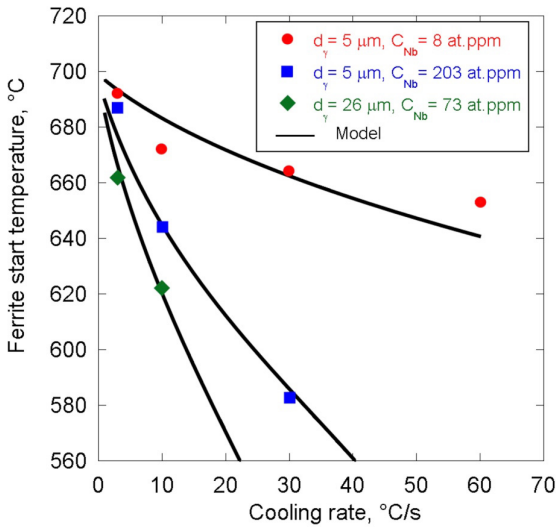


Figure 2. Calculated and measured ferrite transformation start temperature.

The subsequent growth of ferrite is described using the Johnson-Mehl-Avrami-Kolmogorov (JMAK) model and adopting additivity such that the normalized fraction transformed along a cooling path is given by:

$$X = 1 - \exp\left(-\int_T^{T_s} \frac{\beta(T, C_{Nb}, d_\gamma)}{\psi(T)} dT\right)^n \quad (8)$$

Here, ψ is the instantaneous cooling rate, n is the JMAK exponent and the rate parameter β can be written as:

$$\beta = \exp(\beta_1 T + \beta_2 / d_\gamma^{\beta_3}) \quad (9)$$

where the β_i are taken to be linear functions of the amount of Nb in solution, i.e.:

$$\beta_i = \beta_{i1} C_{Nb} + \beta_{i2} \quad (10)$$

Table V gives the JMAK parameters for ferrite growth. The true fraction of ferrite, X_α , is obtained by dividing the normalized fraction with the ferrite equilibrium fraction for the respective transformation temperature.

Table V. JMAK Parameters for Ferrite Transformation*

n	β_{11}	β_{12}	β_{21}	β_{22}	β_{31}	β_{32}
1.1	5.27×10^{-5}	-3.59×10^{-2}	-4.64×10^{-2}	24.9	1.97×10^{-4}	5.98×10^{-2}

*when T is in °C, d_γ in μm and C_{Nb} in at.ppm

In order to incorporate the bainite portion of the transformation into the model it is required to determine the start of the bainite formation. There are two scenarios: (i) bainite forms without prior ferrite formation, (ii) bainite forms after initial ferrite formation. In case (i) the bainite start temperature, B_S , is higher than the calculated ferrite start temperature, T_S . The criterion for measurable bainite start without prior ferrite formation is then given by the 5 % threshold for the fraction transformed such that:

$$0.05 = \int_{B_N}^{B_S} \frac{b_1 + b_2 T}{1 + b_3 C_{Nb}} \frac{dT}{\psi} \quad (11)$$

provides an empirical criterion for B_S where the b_i are empirical constants and B_N is the bainite nucleation temperature that can be related to a critical driving pressure as originally proposed by Ali and Bhadeshia [34]. For the investigated steel $B_N = 640$ °C as long as there is no prior ferrite

formation (i.e. $X_\alpha=0$). Table VI summarizes the bainite start parameters and Figure 3 illustrates the quality of the bainite start model by comparing calculations with measured data.

Table VI. Bainite Start Parameters

$b_1(s^{-1})$	$b_2(s^{-1} \cdot ^\circ C^{-1})$	$b_3(at.ppm^{-1})$
87	-0.132	2.1

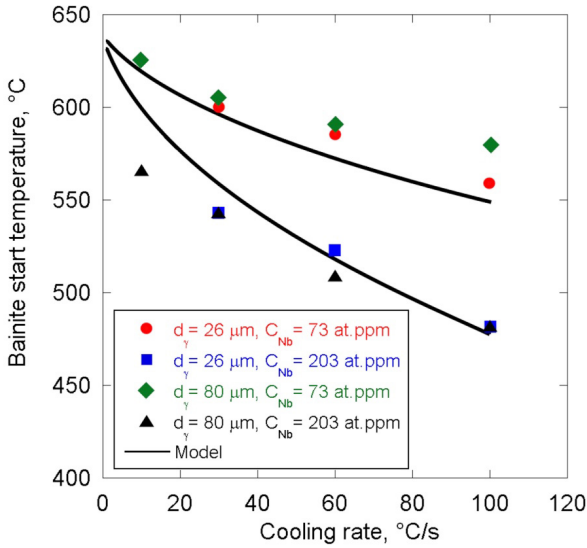


Figure 3. Calculated and measured bainite transformation start without prior ferrite formation.

In case (ii), i.e. when there is prior ferrite formation, B_N provides the condition for the cessation of ferrite formation and onset of bainite transformation. The driving pressure for the austenite-ferrite formation is both a function of temperature and carbon content of austenite. The latter depends on the degree of ferrite formation such that the critical driving pressure for B_N ($^\circ C$) can be expressed as a function of ferrite fraction. For the present steel, the following relation is obtained:

$$B_N = 640 - 143X_\alpha^{1/2} + 288X_\alpha - 528X_\alpha^2 + 646X_\alpha^3 - 380X_\alpha^4 \quad (12)$$

where X_α is the ferrite fraction at B_N and represents then the final ferrite fraction.

Subsequent bainite growth, i.e. starting from B_S when $X_\alpha=0$ and from B_N when $X_\alpha>0$, is described using the JMAK approach outlined by equations (8 - 10). The JMAK parameters depend on whether or not prior ferrite formation had taken place, as summarized in Table VII. The normalization factor to obtain the true fraction, X_B , of bainite is $(1-X_\alpha-X_{MA})$ where X_{MA} is the MA fraction that can be related to the transformation start temperature Θ_S (i.e. either T_S for $X_\alpha>0$ or B_S for $X_\alpha=0$) in °C by:

$$X_{MA} = 0.0604 + \frac{0.0144 - 0.0604}{1 + \exp((\Theta_S - 593)/2.65)} \quad (13)$$

as shown in Figure 4.

Table VII. JMAK Parameters for Bainite Transformation*

X_α	n	β_{11}	β_{12}	β_{21}	β_{22}	β_{31}	β_{32}
0	1.1	6.88×10^{-6}	-2.34×10^{-2}	-2.47×10^{-2}	18.0	2.40×10^{-4}	1.17×10^{-1}
> 0	1.1	7.64×10^{-6}	-2.36×10^{-2}	-1.22×10^{-2}	12.5	0	0

*when T is in °C, d_γ in μm and C_{Nb} in at.ppm

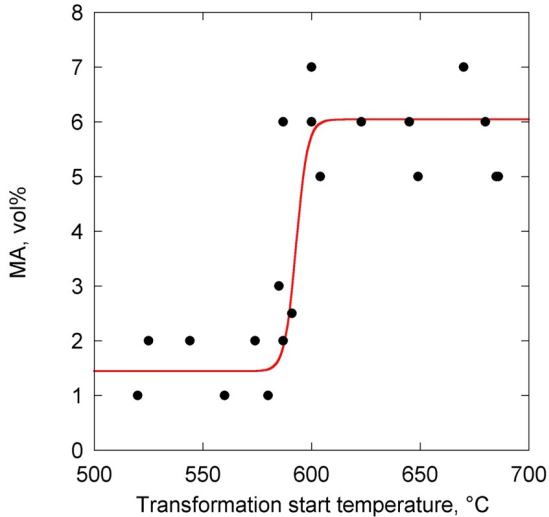


Figure 4. Martensite/Austenite (MA) fraction as a function of transformation start temperature during continuous cooling transformation; solid line represents equation (13).

Figure 5 gives examples for comparing the overall transformation model (i.e. kinetics of the ferrite and bainite portions) with experimentally observed transformation kinetics during continuous cooling. The three examples are representative cases for a reaction that produces a primarily ferrite microstructure (highest transformation temperature), a reaction where bainite transformation dominates and no ferrite forms (lowest transformation temperature) as well as a case where a mixture of ferrite and bainite is observed (intermediate transformation temperature).

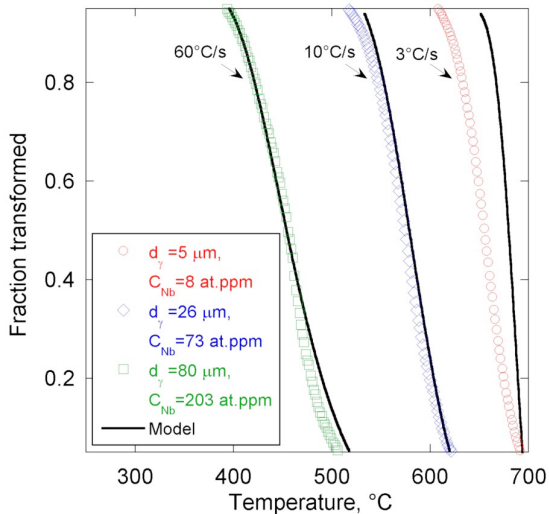


Figure 5. Comparison of calculated and measured transformation kinetics during continuous cooling from various austenizing conditions.

Model Validation

The above described model presents an integrated microstructure model for austenite grain growth and austenite decomposition in the investigated X80 linepipe steel. In formulating the model heating and cooling conditions were considered that are of relevance for the HAZ. To assess the predictive capabilities of the model for the HAZ a series of laboratory simulations were performed using potential HAZ thermal cycles according to the Rosenthal equation for thick plates, i.e.:

$$T(t,r) = T_o + \frac{q}{2\pi\kappa vt} \exp\left(-\frac{q}{2e\pi\kappa vt} \frac{1}{(T_{peak}(r) - T_o)}\right) \quad (14)$$

Here, t is time, r is the distance from the fusion line, v is the weld speed, q is the heat input, κ ($=40 \text{ J/msK}$) is the thermal conductivity, T_o is the pre-heat temperature and the peak temperature is given by:

$$T_{peak} = T_o + \frac{2q/v}{\pi e \rho r^2} \quad (15)$$

where ρ ($=4.68 \times 10^6 \text{ J/m}^3\text{K}$) is the volume heat capacity. According to eq. (14) the cooling time from 800 to 500°C is given by:

$$\Delta t_{8-5} = \frac{q/v}{2\pi\kappa} \left(\frac{1}{500 - T_o} - \frac{1}{800 - T_o} \right) \quad (16)$$

where T_o is in °C. For simplicity a heating rate of 100 °C/s was employed in the validation tests to reach the peak temperature. The studies of Banerjee et al. [2] had indicated that the austenite grain size becomes independent of heating rate when the heating rate is 100 °C/s and higher. Three thermal cycles were employed with different peak temperatures, i.e. here 1000, 1200 and 1350 °C, that according to eq. (15) represent different positions in the HAZ. An idealized Rosenthal behaviour ($q/v=1.04 \text{ kJ/mm}$, $T_o=330 \text{ °C}$) was assumed for the cooling portion such that the cooling time from 800 to 500 °C is approximately 16 s which translates into an average cooling rate through the transformation region of 19 °C/s. Figure 6 summarizes the time-temperature paths of the employed thermal cycles.

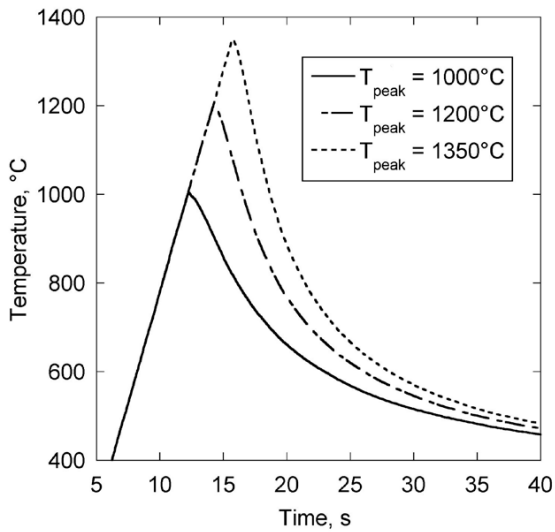


Figure 6. Simulated HAZ thermal cycles employed for model validation studies.

Figure 7 shows the final microstructures obtained for these three different heat treatment cycles. For a peak temperature of 1000 °C a predominantly ferritic microstructure is observed. Increasing the peak temperature leads to an increasingly bainitic microstructure such that for a peak temperature of 1350 °C a completely bainitic microstructure is recorded.

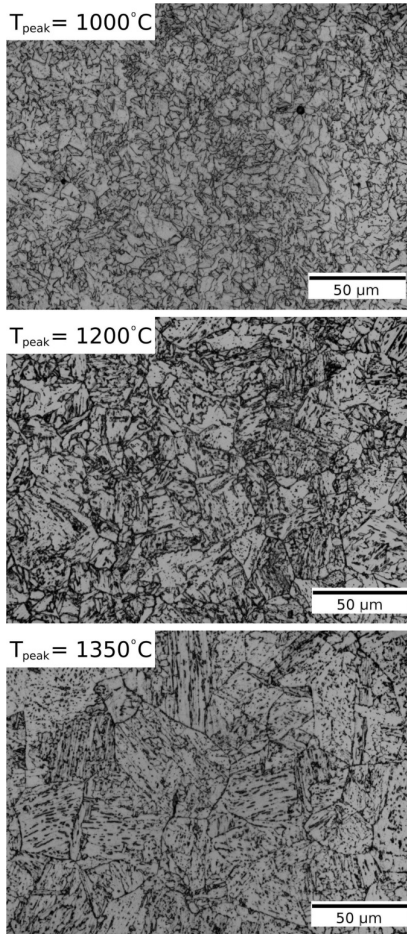


Figure 7. Final microstructures obtained during simulated HAZ thermal cycles with different peak temperatures.

The combined microstructure model was then applied to these three thermal cycles. Table VIII indicates the predicted austenite condition in terms of grain size and amount of Nb in solution. It can be observed that increasing the peak temperature clearly results in an increase of both austenite grain size and Nb in solution. Further, Table VIII provides the comparison of predicted and measured fractions of transformation products. The trends observed in the laboratory tests are adequately predicted by the model. In detail, it appears that the fraction of the MA

constituent is in general somewhat underpredicted. This may, at least in part, be attributable to the fact that an empirical relationship has been employed for the MA fraction and experimental data points show significant scatter with respect to the proposed fit (see Figure 4). Further, it is challenging to accurately measure the MA fraction as some of the MA islands can be rather small. This may be another contributing factor to the observed discrepancies. While a potentially improved MA model will be useful it will have minor effects on the overall transformation model as the MA fraction remains below 0.10 in all cases, i.e. the transformation is dominated by the ferrite and/or bainite reactions.

Table VIII. Predicted Austenite Condition and Predicted and Measured Fractions of Transformation Products

T_{peak} (°C)	C_{Nb} (at.ppm)	d_γ (μm)	X_α (pred.)	X_α (meas.)	X_B (pred.)	X_B (meas.)	X_{MA} (pred.)	X_{MA} (meas.)
1000	8	4	0.94	0.90	0	0	0.06	0.10
1200	63	11	0.06	0.10	0.88	0.82	0.06	0.08
1350	204	35	0	0	0.98	0.95	0.02	0.05

Conclusions

A phenomenological modelling framework has been developed to describe austenite grain growth, dissolution of precipitates and austenite decomposition into ferrite and bainite along rapid heat treatment cycles that are typical for the HAZ. The integrated microstructure model has been validated for an X80 linepipe steel with laboratory simulations of heat treatment cycles representing different positions in the HAZ. The model is applicable to the portion of the HAZ that experiences complete austenitization with promising predictive capabilities in terms of the fraction of transformation products as a function of the distance from the fusion line.

There are a number of points that should be considered for improving and extending the model.

- (1) The microstructure model needs to be connected to a structure-property model to predict the mechanical properties of the HAZ, in particular fracture toughness. For this purpose it will be required to develop structure-property relationships that can be applied to individual positions in the HAZ and subsequently will be integrated over the graded microstructure of the HAZ.
- (2) The MA constituent is an important microstructure aspect for crack propagation and, thus, the fracture behaviour of the HAZ. The current model makes rather approximate predictions for the MA fraction. It is imperative to improve the quality of the MA fraction model and to add a component to predict the size of the MA constituent. The MA size critically determines whether or not the MA constituent will promote crack propagation. It can be expected that sufficiently small MA islands are inconsequential as long as they are smaller than the critical crack length. Other important characteristics of MA constituents are their morphology and carbon content.
- (3) The current model deals with the HAZ portion that is completely austenitized. An extension to the intercritical region would be of interest but requires the development of an austenite formation model. For most welding scenarios, the thickness of the

intercritical region is expected to be sufficiently small such that it may not affect the HAZ properties significantly.

- (4) The HAZ is characterized by steep temperature gradients that result in associated microstructure gradients. The present model makes predictions for individual portions in the HAZ without accounting for these gradients, i.e. the thermal cycle of this position is applied to the microstructure evolution as if it were to occur in a bulk sample with homogeneous temperature. For example, immediately near the fusion line austenite grains with sizes of approximately 100 μm may be present and even a conservative estimate would suggest that there may be a temperature gradient of at least 200 $^{\circ}\text{C}$ across a grain of this size. Thus, modelling microstructure evolution on the length scale of the grain structure, i.e. the so-called meso-scale, will be important to account for the potential effects of these temperature gradients on the resulting microstructure. It is proposed to translate the presented model into a phase field model (PFM). Initial PFM simulations have been carried out for austenite grain growth in the HAZ [35].

Acknowledgement

We acknowledge the financial support received from the Natural Sciences and Engineering Research Council of Canada, Evraz Inc. NA and TransCanada Pipelines Ltd. with gratitude. Further, we would like to thank Jennifer Reichert for her assistance in analyzing continuous cooling transformation data.

References

1. M. Militzer, "Computer Simulation of Microstructure Evolution in Low Carbon Sheet Steels," *ISIJ International*, 47 (2007), 1-15.
2. K. Banerjee et al., "Nonisothermal Austenite Grain Growth Kinetics in a Microalloyed X80 Linepipe Steel," *Metallurgical and Materials Transactions A*, 41 (A) (2010), 3161-3172.
3. M. Maalekian et al., "In Situ Measurement and Modelling of Austenite Grain Growth in a Ti/Nb Microalloyed Steel," *Acta Materialia*, 60 (2012), 1015-1026.
4. R.I.L. Guthrie and J.J. Jonas, *ASM Handbook Volume 1: Properties and Selection: Irons, Steels and High-Performance Alloys*, 10th edition (Materials Park, OH: ASM International, 1990), 115-116.
5. M. Militzer et al., "Austenite Grain Growth Kinetics in Al-Killed Plain Carbon Steels," *Metallurgical and Materials Transactions A*, 27 (A) (1996), 3399-3409.
6. K. Easterling, *Introduction to the Physical Metallurgy of Welding* (Oxford, UK: Butterworth-Heinemann Ltd., 1992)
7. L.P. Zhang, C.L. Davis and M. Strangwood, "Effect of TiN Particles and Microstructure on Fracture Toughness in Simulated Heat-Affected Zones of a Structural Steel," *Metallurgical and Materials Transactions A*, 30 (A) (1999), 2089-2096.

8. M. Eroglu and M. Aksoy, "Effect of Initial Grain Size on Microstructure and Toughness of Intercritical Heat-Affected Zone of a Low Carbon Steel," *Materials Science and Engineering A*, A286 (2000), 289-297.
9. S. Kou, *Welding Metallurgy*, 2nd edition (New Jersey, NJ: John Wiley & Sons Inc., 2003)
10. M.F. Ashby and K.E. Easterling, "A First Report on Diagrams for Grain Growth in Welds," *Acta Materialia*, 30 (1982), 1969-1978.
11. J.C. Ion, K.E. Easterling and M.F. Ashby, "A Second Report on Diagrams of Microstructure and Hardness for Heat-Affected Zones in Welds," *Acta Materialia*, 32 (1984), 1949-1962.
12. S. Mishra and T. DebRoy, "Non-Isothermal Grain Growth in Metals and Alloys," *Materials Science and Technology*, 22 (2006), 253-278.
13. J. Moon, J. Lee and C. Lee, "Prediction for the Austenite Grain Size in the Presence of Growing Particles in the Weld HAZ of Ti-Microalloyed Steel," *Materials Science and Engineering A*, 459 (2007), 40-46.
14. I. Andersen and O. Grong, "Analytical Modelling of Grain Growth in Metals and Alloys in the Presence of Growing and Dissolving Precipitates - I. Normal Grain Growth," *Acta Metallurgica et Materialia*, 43 (1995), 2673-2688.
15. C. Henwood et al., "Coupled Transient Heat Transfer - Microstructure Weld Computations (Part B)," *Acta Metallurgica*, 36 (1988), 3037-3046.
16. H.K.D.H. Bhadeshia, L.E. Svensson and B. Grefott, "A Model for the Development of Microstructure in Low-Alloy Steel (Fe-Mn-Si-C) Weld Deposits," *Acta Metallurgica*, 33 (1985), 1271-1283.
17. S.S. Babu, "Thermodynamic and Kinetic Models for Describing Microstructure Evolution During Joining of Metals and Alloys," *International Materials Reviews*, 54 (2009), 333-367.
18. O. Grong, *Metallurgical Modeling of Welding, Materials Modeling Series* (London, UK: Institute of Materials, 1997)
19. W. Zhang, J.W. Elmer and T. DebRoy, "Integrated Modelling of Thermal Cycles, Austenite Formation, Grain Growth and Decomposition in the Heat Affected Zone of Carbon Steel," *Science and Technology of Welding and Joining*, 10 (2005), 574-582.
20. H.K.D.H. Bhadeshia and L.E. Svensson, "Modelling the Evolution of Microstructure in Steel Weld Metal" *Mathematical Modelling of Weld Phenomena, Volume 1*, editors H. Cerjak and K. Easterling (London, UK: Institute of Materials, 1993), 109-182.

21. R.G. Thiessen, I.M. Richardson and J. Sietsma, "Physically Based Modelling of Phase Transformations During Welding of Low-Carbon Steel," *Materials Science and Engineering A*, 427 (2006), 223-231.
22. F. Fazeli et al., "Modeling the Effect of Nb on Austenite Decomposition in Advanced Steels," *The International Symposium on the Recent Developments in Plate Steels* (Warrendale, PA: AIST, 2011), 343-350.
23. F. Fazeli and M. Militzer, "Effect of Nb on Austenite Formation and Decomposition in an X80 Linepipe Steel," *Journal of Iron and Steel Research, International*, 18, Supplement 1-2 (2011), 658-663.
24. M. Perez, "Gibbs–Thomson Effects in Phase Transformations," *Scripta Materialia*, 52 (2005), 709-712.
25. F.J. Humphreys and M. Hatherly, *Recrystallization and Related Annealing Phenomena*, 2nd edition (Oxford, UK: Elsevier Ltd, 2004)
26. M. Hillert, "On the Theory of Normal and Abnormal Grain Growth," *Acta Metallurgica*, 13 (1964), 227-238.
27. P.R. Rios, "Overview no. 62: A Theory for Grain Boundary Pinning by Particles," *Acta Metallurgica*, 35 (1987), 2805-2814.
28. S. Uhm et al., "Prediction Model for the Austenite Grain Size in the Coarse Grained Heat Affected Zone of Fe-C-Mn Steels: Considering the Effect of Initial Grain Size on Isothermal Growth Behavior," *ISIJ International*, 44 (2004), 1230-1237.
29. J. Friedberg, L.E. Törm Dahl and M. Hillert, "Diffusion in Iron," *Jernkontorets Ann.*, 153 (1969), 263-276.
30. Thermodynamic Database 'mc_steel' (version 1.86), Diffusion Database 'mc_sample_fe' (version 1.03) Institute of Materials Science and Technology, Vienna University of Technology, Austria.
31. M. Militzer, R. Pandi and E.B. Hawbolt, "Ferrite Nucleation and Growth During Continuous Cooling," *Metallurgical and Materials Transactions A*, 27 (A) (1996), 1547-1556.
32. M. Militzer, F. Fazeli and H. Azizi-Alizamini, "Modelling of Microstructure Evolution in Advanced High Strength Steels," *La Metallurgia Italiana*, 4 (2011), 35-41.
33. S.S. Babu and H.K.D.H. Bhadeshia, "Diffusion of Carbon in Substitutionally Alloyed Austenite," *Journal of Materials Science Letters*, 14 (1995), 314-316.
34. A. Ali and H.K.D.H. Bhadeshia, "Nucleation of Widmanstätten Ferrite," *Materials Science and Technology*, 6 (1990), 781-784.

35. M. Toloui and M. Militzer, "Phase Field Simulation of Austenite Grain Growth in the HAZ of Microalloyed Linepipe Steel," *International Journal of Materials Research*, 101 (2010), 542-548.